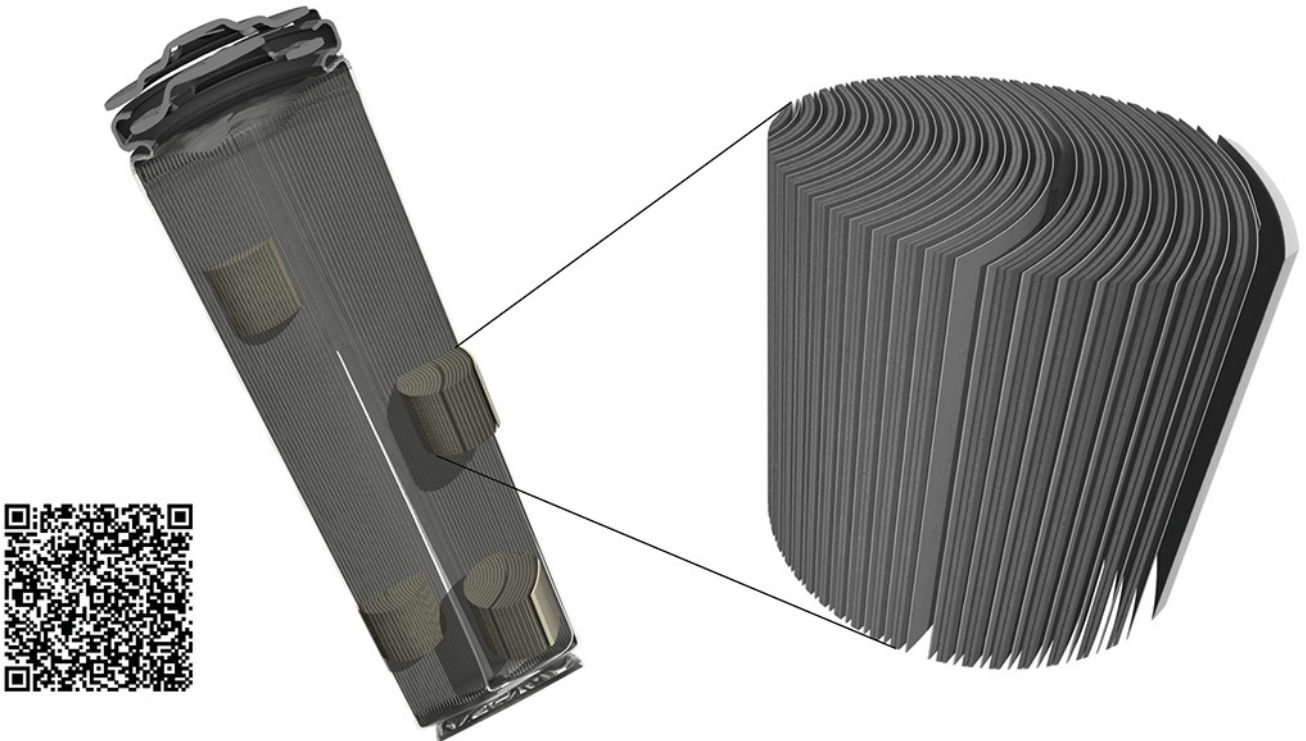


TESCAN micro-CT solutions

for energy storage materials research



TESCAN UniTOM XL

- ✓ Multi-scale non-destructive 3D imaging optimized to maximize throughput and contrast
- ✓ Fast scanning and high sample throughput with temporal resolutions below 10 seconds
- ✓ Wide array of samples types
- ✓ Enables dynamic tomography and *in-situ* experiments
- ✓ Dynamic screening for synchrotron beamtime
- ✓ Modular and open system with unmatched flexibility for research



[Click and find out more](#)

Achieving Ultrarobust and Humidity-Resistant Triboelectric Nanogenerator by Dual-Capacitor Enhancement System

Linglin Zhou, Yikui Gao, Di Liu, Li Liu, Zhihao Zhao, Shaoxin Li, Wei Yuan, Shengnan Cui, Zhong Lin Wang,* and Jie Wang*

Triboelectric nanogenerators (TENGs) that can efficiently harvest ubiquitous mechanical energy provide a promising technology for the energy supply of intelligent electronic devices. However, the issues of low durability induced by wear and moisture sensibility of TENGs greatly limit their practical applications. Here, a no-wear dual-capacitor enhancement system (DCES) to simultaneously improve the service lifetime and electric performance of TENGs in a high humidity environment is proposed. The combination of low charge injection from lightly touched TENG and charge transfer in no-wear DCES can synchronously realize ultralow material wear and charge pumping up. Therefore, the dual-capacitor-enhanced TENG (DCE-TENG) achieves a long service life of at least 1 000 000 cycles with 15-fold enhancement of matched average power. Furthermore, owing to the humidity resistance of DCES, the output performance of DCE-TENG remains 95% of the initial value in 90% humidity. This work is expected to promote the commercial applications of TENGs.

features of light weight, material variety, easy fabrication, low cost, and high efficiency at low operation frequency,^[6,7] TENG has been verified as an efficient energy harvesting technology for applications in micro-/nanopower source,^[8] self-powered sensor,^[9] blue energy harvester,^[10] and high-voltage source.^[11] To promote the commercialization and application of TENG, numerous efforts have been devoted to elevating the surface charge density of TENG, such as material selection,^[12] structure design,^[13] ion injection,^[14] and environmental control.^[15] Recently, charge pumping and charge excitation strategy combined with ultrathin dielectric film were proposed to break through the limitation of air breakdown,^[16–19] and thus boosted the charge density to a record

value of 2.38 mC m^{-2} .^[18] Nevertheless, the charge pumping and charge excitation strategy are primarily well applicable for contact–separation mode TENG (CS-TENG), which is sensitive to humidity due to its adverse impact on electron transfer process in TENG.^[20]

To achieve humidity-resistant TENG, many research works have been carried out for enhancing the output performance of CS-TENG in high humidity environment by using packaging technique^[21] or superhydrophobic friction surface.^[22] Due to the smaller gap distance in friction interface, sliding mode TENG (S-TENG) has been reported as a simple strategy to improve the output performance of TENG in high ambient humidity due to it being less negatively affected by humidity compared to CS-TENG.^[23] Furthermore, compared to CS-TENG, S-TENG exhibits the high conversion efficiency such that a saturation surface charge density can be obtained after triboelectrification within several operation cycles,^[24] where only electrostatic induction process is necessary to generate output in the following operation when there is no charge loss. However, due to the high charge dissipation of TENG in atmosphere, a continuous violent friction is always employed to obtain a high output performance, which will cause serious material wear and thus poor durability. Although some strategies including noncontact mode,^[25] rotational contact–separation mode,^[26] and auto-mode-transition^[27] have been reported to reduce mechanical wear and improve the service life of S-TENG to some extent, it is difficult to achieve a high output performance at the same time due to the low triboelectrification effect. Inspired by the equivalent physical model of TENG that is represented by an

1. Introduction

With the rapid development of internet of things, sensor networks, big data, robotics, and artificial intelligence, the demand of clean, sustainable, and distributed power source increases dramatically.^[1–4] To address this issue, triboelectric nanogenerator (TENG) was invented to harvest mechanical energy from ubiquitous mechanical motions.^[5] Owing to the unique

L. Zhou, Y. Gao, D. Liu, L. Liu, Z. Zhao, S. Li, W. Yuan, S. Cui, Z. L. Wang, J. Wang

Beijing Institute of Nanoenergy and Nanosystems
Chinese Academy of Sciences
Beijing 101400, P. R. China

E-mail: zhong.wang@mse.gatech.edu; wangjie@binn.cas.cn


L. Zhou, D. Liu, Z. Zhao, S. Li, W. Yuan, S. Cui, Z. L. Wang, J. Wang
School of Nanoscience and Technology
University of Chinese Academy of Sciences
Beijing 100049, P. R. China

Y. Gao

Center on Nanoenergy Research
School of Physical Science and Technology
Guangxi University
Nanning 530004, P. R. China

Z. L. Wang

School of Materials Science and Engineering
Georgia Institute of Technology
Atlanta, GA 30332, USA

 The ORCID identification number(s) for the author(s) of this article can be found under <https://doi.org/10.1002/aenm.202101958>.

DOI: 10.1002/aenm.202101958

ideal voltage source and a variable capacitance,^[28] developing no-wear variable capacitance to utilize the energy output from TENG instead of electrostatic induction that is usually accompanied by material wear for generating electricity is highly desired to avoid the invalid friction after reaching a saturation output, and thus eliminates the mechanical wear without sacrificing the electrical output performance.

In this work, we report a no-wear dual-capacitor enhancement system (DCES) to prolong the service life and boost the electric output of TENG in a wide range of humidity. As for the dual-capacitor-enhanced TENG (DCE-TENG), charge injected from TENG transfers in no-wear DCES instead of electrostatic induction to produce electricity in external circuit. Due to a low leakage current of DCES, a low output of TENG with slight contact can satisfy the charge replenishment of the system, and thus boost the output of DCE-TENG. Attributing to the slightly contact mode TENG and no-wear DCES, the

DCE-TENG delivers a long-term life with 94% of charge retention after 1 000 000 cycles, and the maximum average power of DCE-TENG enhances by 15 times compared to TENG. More importantly, without the influence of humidity on the capacitance of DCES and thus charge transferring, DCE-TENG exhibits a superior humidity resistance, where 95% retention value under 90% humidity is achieved. This work provides an efficiency strategy of improving both the durability and electric output performance of TENG at high humidity environment.

2. Results and Discussion

2.1. Structure Design and Working Mechanism of DCE-TENG

The basic structure of DCE-TENG is displayed in **Figure 1a**, which mainly consists of a rotary freestanding mode TENG (TENG),

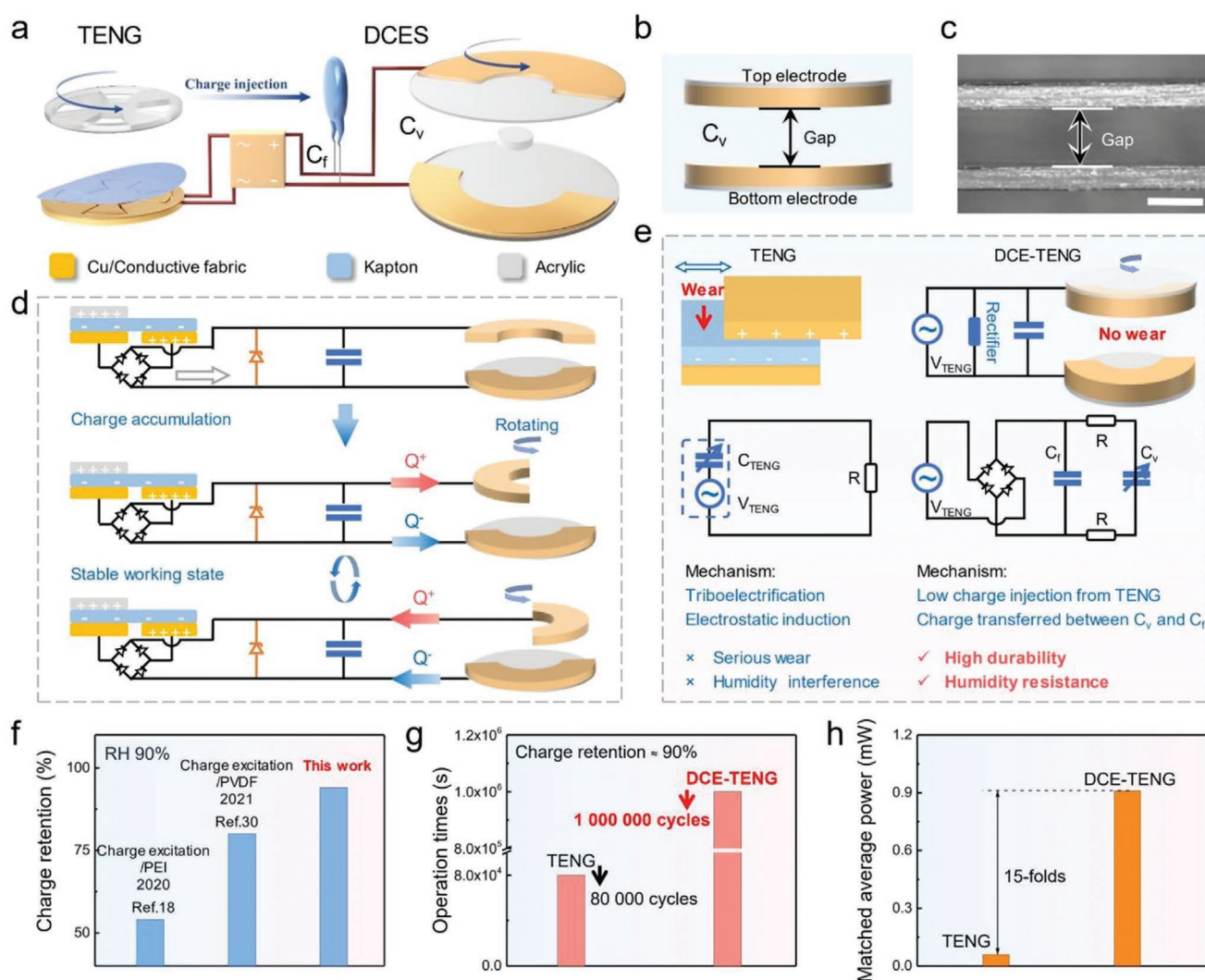


Figure 1. Structure design and working mechanism of DCE-TENG. a) Structural schematic of DCE-TENG. b) Structural schematic and c) optical microscopy image of the gap distance between electrodes of C_v (scale bar: 1 mm). d) Working mechanism of DCE-TENG. e) Comparison of working mechanism of DCE-TENG with traditional TENG. f) Comparison of humidity resistance of DCE-TENG with different type performance-enhanced TENGs through charge pump strategy. g) The durability of DCE-TENG compared to traditional TENG. h) Comparison of matched average power of DCE-TENG with normal TENG.

a rectifier, and a DCES including a designed variable capacitor (C_v) and a commercial ceramic capacitor as fixed capacitor (C_f). The TENG is composed of a rotator and a stator (Figure S1a,b, Supporting Information), which uses acrylic and Kapton film for the tribomaterials, and conductive fabric for the complementary electrodes. The C_v is made up of two semicircular-type electrodes (Figure S1c,d, Supporting Information) pasted by Kapton film, between which there is a certain gap distance created by a spacer to avoid direct contact, as depicted in the right part of Figure 1a. The gap distance between the two electrodes is about 1 mm (Figure 1b,c), which can achieve no mechanical wear due to the noncontact friction surface. Here, ten units are connected in parallel to elevate the maximum capacitance of C_v (Figure S1e, Supporting Information).

Different from the working mechanism of previous reported works using charge pumping method,^[16–19,29] the output of DCE-TENG is achieved by the charge transfer inner the DCES, and the corresponding detailed working process is depicted in Figure 1d. In charge accumulation process, the external TENG injects charges into the DCES through a rectifier. Then, by rotating the top electrode of C_v , its capacitance changes from zero to the maximum value when the overlapping area of the electrode pair varies from the minimum to the maximum, while the C_f keeps a constant value, resulting in a voltage difference between them. Therefore, the charge will transfer between the C_v and C_f , producing an alternative current in external circuit.

The comparison of physical and electric model of DCE-TENG with traditional TENG is displayed in Figure 1e. Traditional TENG is based on the coupling effect of triboelectrification and electrostatic induction, where a continuous violent friction in the following electrostatic induction that is not necessary but often used will cause material wear, and thus lead to a decrease in durability of TENG. Besides, the operation of TENG sensitively depends on moisture which greatly affects the process of electron transfer. Unlike the conventional TENG, the working mechanism of DCE-TENG is based on the couple processes of low charge injection from TENG and charge transferred between no-wear C_v and C_f , where TENG with light contact can satisfy the supplementary of small leakage charge of DCES when the system reaches a stable working state. Noteworthily, the value of C_v exhibits much less sensitivity to the influence of moisture compared to triboelectrification and electrostatic induction process, which will improve the humidity resistance of the designed DCE-TENG.

The development of humidity resistance in TENG through improving charge accumulation process is depicted in Figure 1f. Under the relative humidity of 90%, only 54% output was retained for the charge excitation mode TENG.^[18] By adopting polyvinylidene fluoride as friction layer to achieve fast charge accumulation process, the output of TENG was kept 80% compared to the initial value.^[30] In this work, about 95% output can be maintained for DCE-TENG, which is almost impervious to the high humidity environment. In addition, the DCE-TENG also maintains 94% output after 1 000 000 operation cycles, while TENG with violence friction only can operate 80 000 cycles with 90% charge retention (Figure 1g). Thanks to the coupling mechanism of charge pump strategy and the characteristic of variable capacitor, the maximum average power of

DCE-TENG enhances by 15 times compared to external TENG (Figure 1h).

2.2. Critical Factors for the Output Performance of DCE-TENG

The basic electric performances of DCE-TENG are shown in Figure 2. A Zener diode with stabilized voltage of 600 V was adopted to stabilize the voltage and ensure a stable output. The transferred charge of TENG is 80 nC (Figure 2a), and the corresponding short-circuit current and open-circuit voltage are 0.3 μ A and 1600 V (Figure 2b and Figure S2 (Supporting Information)), which is enough to charge the DCES. With charge injection from TENG, the transferred charge of DCE-TENG increases at first, and then reaches a stable value under an operation frequency of 1 Hz (Figure 2c). Here, a C_f with 50 nF and C_v with maximum capacitance of 1.0 nF were adopted, and the stable value of DCE-TENG reaches to 568 nC, which is 6.8 times compared to the external TENG. The corresponding stable current is 1.25 μ A as displayed in Figure S3 (Supporting Information), and the capacitance of C_v with different overlapping areas of the two electrodes is depicted in Figure S4 (Supporting Information). It is worth noting that the transferred charge of C_v is only 28 nC (Figure S5, Supporting Information), which is far less than that of DCE-TENG. Therefore, the output of C_v has a negligible effect on the output performance of DCE-TENG system.

Besides, the critical factors for the output performance of DCE-TENG were examined. From the circuit diagram (Figure 1d), the voltages of C_v and C_f are always equal. Based on parallel-plate model, as the capacitance of C_v changes, the transferred charge (ΔQ) of DCE-TENG in different states is displayed and discussed in detail in Figure 2d and Note S1 (Supporting Information), which can be briefly derived and expressed by

$$\Delta Q = \frac{C_v C_f V_0}{(C_v + C_f)} \quad (1)$$

where C_v and C_f are the capacitances of C_v and C_f , and V_0 is the voltage offered by TENG. It is easy to find that ΔQ is dependent on C_v , C_f , and V_0 . To investigate the influence of the relationship between C_v and C_f in ΔQ , we define an equation as follows

$$C_f = x C_{v \max} \quad (2)$$

$C_{v \max}$ is the maximum value of C_v when the top electrodes and bottom electrodes are completely overlapping. When the top electrodes of C_v rotate 180° from working state i to state iii, the capacitance of C_v varies from zero to the maximum value of 1 nF, and then the maximum ΔQ (ΔQ_{\max}) can be obtained after the stored charge in C_f transfers to C_v , which can be expressed by

$$\Delta Q_{\max} = \frac{x}{x+1} V_0 C_{v \max} \quad (3)$$

Here, V_0 is equal to the stabilized voltage of Zener diode with 600 V. According to Equation (3), the impact of relationship between C_v and C_f on transferred charge of DCE-TENG can

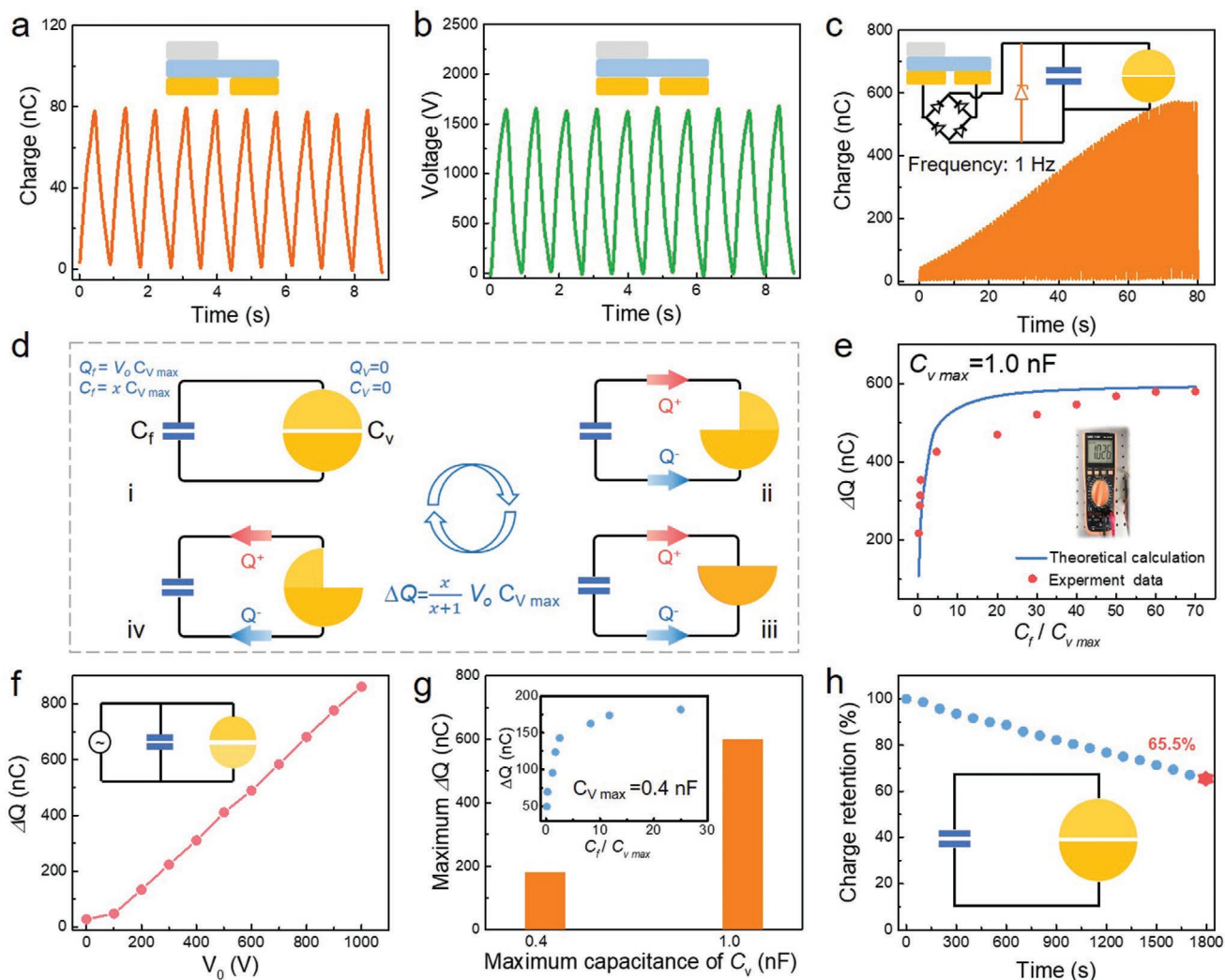


Figure 2. Critical factors for the output performance of DCE-TENG. a,b) Charge and open-circuit voltage of TENG. c) Charge accumulation process of DCE-TENG with voltage stabilization element under 1 Hz operation frequency. d) Charge transferred between the C_v and C_f . e) Maximum charge transfer with the relationship between C_v and C_f . f) Charge of the DCES under different initializing voltages. g) The influence of maximum capacity of C_v on the maximum transferred charge of DCE-TENG, inset is the charge transfer of DCE-TENG with 0.4 nF $C_{v \max}$ under different C_f . h) Charge decay of the charged DCES after removing the TENG.

be depicted in Figure 2e. On the basis of theoretical calculation (blue line), under a fixed capacitance of C_v , the transferred charge first rises with increasing the value of C_f , and then reaches a stable value. The tendency of experiment data (red dots) is very close to the results of theoretical calculation, demonstrating that a maximum transferred charge of DCE-TENG can be realized when the ratio of C_f and C_v is larger than 20.

To investigate the effect of V_0 on the output performance of DCE-TENG, a constant voltage source was applied to control V_0 . Clearly, the transferred charge of DCE-TENG linearly rises with the increasing of V_0 within the range of 0–1000 V (Figure 2f), indicating that DCE-TENG can work within this range without air breakdown. More importantly, the $C_{v \max}$ determines its stored charge quantity, and thus decides the maximum transferred charge of DCE-TENG. As the $C_{v \max}$ rises from 0.4 to 1.0 nF, the maximum transferred charge of DCE-TENG increases from 180 to 570 nC (Figure 2g). The above results

indicate that increasing the supplied voltage of V_0 , maximum capacitance of C_v , and the capacitance ratio of C_f and C_v can realize a larger output performance of DCE-TENG. Additionally, the charge decay of DCES caused by leakage charge was also measured after charging by TENG. Without continuous charge injection from TENG, the transferred charge of DCES exhibits a slow decay, where the output charge also remains 65.5% in 1800 s (Figure 2h and Figure S6 (Supporting Information)), proving a highly stable output of the DCES with low charge leakage.

2.3. Humidity Resistance Performance and Durability of the DCE-TENG

Based on low charge injection from TENG and charge transferred between C_v and C_f , the output performance of

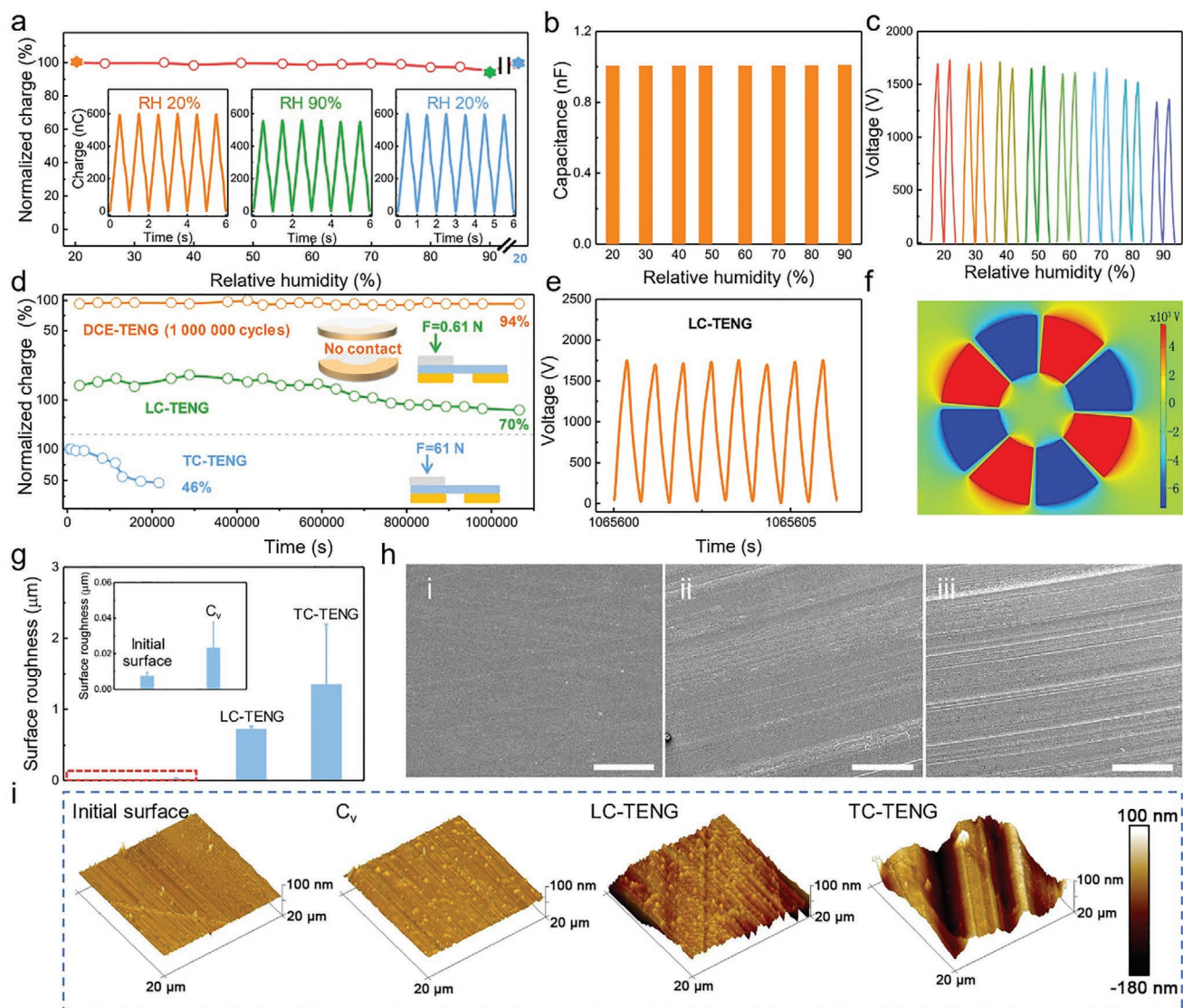


Figure 3. Humidity resistance performance and durability of the DCE-TENG. a) Transferred charge of DCE-TENG, b) the capacitance of C_v , and c) open-circuit voltage of TENG under different humidity. d) Open-circuit voltage of TENG after 1 000 000 s. e) The durability of DCE-TENG after 1 000 000 s at 1 Hz. f) The potential distribution of between the complementary electrodes of TENG. g) Surface roughness of Kapton film at initial state and on different components after 1 000 000 s. h) The SEM images of the dielectric surface of i) C_v , ii) lightly contact mode TENG, and iii) tightly contact mode TENG after 1 000 000 s (scale bar: 500 μm). i) 3D images of dielectric surface corresponding to different samples in (g).

DCE-TENG under various relative humidity conditions is investigated, as shown in **Figure 3a**. As the relative humidity rises from 20% to 90%, the transferred charge of DCE-TENG only declines from 600 to 570 nC, indicating a high retention value of 95% compared to the output under 20% relative humidity. More importantly, the transferred charge quickly returns to its initial value when the relative humidity gets back to 20%. Additionally, the influence of relative humidity on the capacitance of C_v and output performance of TENG is also measured. Clearly, the capacitance of C_v maintains a stable value with the relative humidity varying from 20% to 90% (Figure 3b). Besides, although the open-circuit voltage of TENG exhibits a slightly decline under the high humidity of 90% (Figure 3c), the voltage is still far more than 600 V which is enough to ensure

a stable output of DCE-TENG. The stable value of TENG under different relative humidity might be owing to the continuous contact state of two friction surfaces, and thus greatly reduces the negative effect of high relative humidity. All the above results suggest that due to the less influence of humidity on charge injection from TENG and charge transferring between C_v and C_f , DCE-TENG can work with a stable output even under a high humidity environment.

Moreover, the long-term durability of DCE-TENG was also examined, where a lightly contact mode TENG (LC-TENG) with applied force of 0.61 N is adopted in this work to reduce the material wear of TENG. After 1 000 000 cycles under the frequency of C_v at 1 Hz, DCE-TENG can maintain 94% output compared to its initial state (Figure 3d and Figure S7

(Supporting Information)), suggesting the excellent electric stability of DCE-TENG. Due to the different operation frequency of TENG and C_v , a normalized charge output of DCE-TENG based on LC-TENG and tightly contact mode TENG (TC-TENG, applied force of 61 N, Figure S8, Supporting Information) after long-term operation times are compared to reveal the mechanism of high durability of DCE-TENG. After injecting charge to DCES for 1 000 000 s, the transferred charge of LC-TENG declines to 72 nC (Figure S9, Supporting Information), and the corresponding voltage is 1580 V (Figure 3e). The COMSOL simulation result of potential distribution between the complementary electrodes also demonstrates a high voltage with several thousand volts of TENG after 1 000 000 s (Figure 3f), which is enough to ensure the energy supply for DCES. While for the TC-TENG, although a higher initial output of 394 nC compared to LC-TENG is obtained (Figure S10, Supporting Information), it only maintains 46% after 216 000 s (Figure 3c). Furthermore, the surface roughness, scanning electron microscope (SEM) images, and 3D images of the dielectric film corresponding to different samples are also measured (Figure 3g–i). Due to the noncontact between the electrodes of C_v , the surface roughness of dielectric film on C_v is only 0.02 μm , and mechanical wear can be hardly observed on the dielectric surface. Compared to TC-TENG with serious mechanical wear and a big surface roughness of 1.35 μm , LC-TENG exhibits a less mechanical wear as well as a smaller surface roughness of 0.72 μm . More importantly, the surface roughness of LC-TENG has a smaller error bar compared to the TC-TENG, suggesting more uniform friction of the former. From all the above results, DCE-TENG takes advantage of the coupling effects that LC-TENG with less materials wear for injecting charge to DCES, and charge transferring between the C_f and noncontact mode C_v to generate outputs without any wear, which not only largely prolongs the lifetime of DCE-TENG but also greatly boosts the electric outputs of our designed system.

2.4. Electrical Characteristics and Demonstration of DCE-TENG to Drive Electronic Device

To investigate the electric characteristics of DCE-TENG, its other performances were carried out, as displayed in Figure 4a–c. With the operation frequency of TENG at 0.3 Hz, the transferred charge of DCE-TENG keeps a stable value of 570 nC when the frequency of C_v rises from 1 to 5 Hz, while both the peak current and average current exhibit a linear increase (Figure 4a). The maximum peak current and average current of 6.7 and 5.6 μA are obtained at 5 Hz, respectively. It is worth noting that, when the frequency of C_v increases from 1 to 5 Hz with TENG at a fixed frequency of 0.3 Hz, the transferred charge rate of DCE-TENG improves from 1.17 to 2.76 $\mu\text{C s}^{-1}$ (Figure 4b and Figure S11 (Supporting Information)), which improve 550% and 1433% compared to TENG with 0.18 $\mu\text{C s}^{-1}$. The result indicates that a higher output performance of DCE-TENG can be realized at an ultralow-frequency mechanical motion by using a frequency converter. In addition, the output currents and powers of DCE-TENG and TENG at different resistances from 0.01 to 20 000 $\text{M}\Omega$ are depicted in Figures S12 and S13 (Supporting Information). Clearly, the maximum peak

power of 1.1 mW and average power of 0.91 mW for DCE-TENG are obtained with a matched resistance of 80 $\text{M}\Omega$ at 5 Hz, which are larger than that of TENG with 0.09 mW (peak power) and 0.06 mW (average power) at matched resistance of 5000 $\text{M}\Omega$.

The boosted output performance of DCE-TENG is also demonstrated though driving various electronics compared to TENG. The self-powered system based on DCE-TENG that consists of TENG, C_v , and C_f is shown in Figure 4d, and the circuit diagram of the self-powered system based on TENG is displayed in Figure 4e. By using a full-wave rectifier, both of the DCE-TENG and TENG are connected with a capacitor, whose voltage is monitored through a voltmeter. The voltage curves of different capacitors charged by DCE-TENG compared with that of TENG suggest that DCE-TENG demonstrates a faster charge rate (Figure 4f). Specifically, when the switch K1 is on and K2 is off, the TENG takes 68.7 and 161.4 s for charging 4.7 and 10 μF capacitors to 2 V, while DCE-TENG just needs 1.9 and 4.3 s for charging these two capacitors to the same voltage, demonstrating the 36-fold and 38-fold enhancements compared to TENG. The enhanced electric performance of DCE-TENG is also verified to drive a digital watch with a commercial capacitor (47 μF) as energy storage unit. At the initial stage, when the switch K1 is off and K2 is on, DCE-TENG is out of work, the capacitor drives the digital watch alone, leading to a decline of capacitor voltage with a discharging current of 0.19 μA . When the DCE-TENG sets to work with both switches at on state, the voltage of the capacitor immediately rises with a charging current of 0.64 μA , implying the less consumed charge compared to the charging rate (Figure 4g). As for the TENG, the voltage of capacitor continuously decreases even powered by the TENG (Figure 4h), indicating that TENG cannot drive the normal work of digital watch. The demonstration of the DCE-TENG driving a digital watch has been provided as shown in Movie S1 (Supporting Information). Without external power source, the digital watch can be successfully driven by the DCE-TENG at a low working frequency. The detailed structural schematic and flow diagram of DCE-TENG for harvesting mechanical energy are shown in Figure 4i, mechanical energy such as wind energy and water flow energy can drive the rotary of DEC-TENG through rotation shafts that consist of overdrive gear, and then generate electricity to power external load. In this system, a low output of TENG with slight contact can satisfy the charge replenishment of the system, and thus boost the output of DCE-TENG. Moreover, overdrive gear can convert low frequency from mechanical motions to high frequency rotation of C_v , further enhancing the power output of the system. Owing to the rational design, the DCE-TENG system has achieved the merits of long-term service life and humidity resistance.

3. Conclusion

In summary, we develop a no-wear DCES to improve the durability and electric output performance of TENG under high humidity. Composed of a noncontact C_v and C_f , the DCES exhibits the excellent characteristics of no mechanical wear and being insensitive to humidity. Inspired by the working mechanism of TENG based on the triboelectrification and

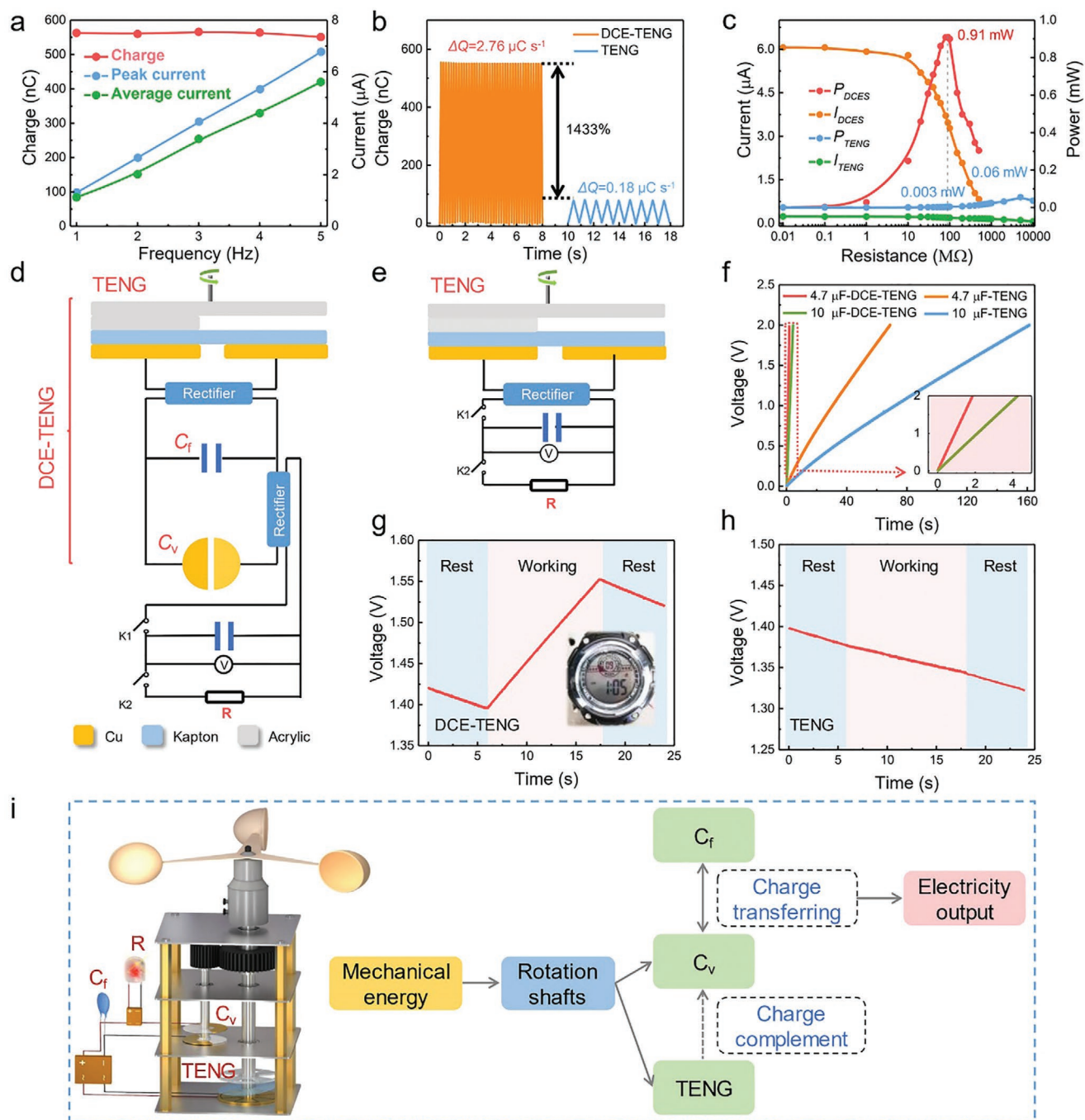


Figure 4. Electrical characteristics and demonstration of DCE-TENG. a) Charge and short-circuit current of DCE-TENG under different frequencies. b) Comparison of transferred charge rate between TENG and DCE-TENG at 5 Hz. c) Average power of the TENG and DCE-TENG under various loads. d) Electric scheme of DCE-TENG and e) TENG for driving electronic device. f) Charging curve of 4.7 and 10 μF capacitor using DCE-TENG and TENG, respectively. g, h) Charging curve of the supercapacitor when a digital watch is driven by (g) DCE-TENG and (h) TENG, respectively. i) Structural schematic and flow diagram of DCE-TENG for harvesting mechanical energy.

electrostatic induction, dual-capacitor-enhanced TENG (DCE-TENG) applies the electric output of TENG as charge source, and adopts charge transferring in DCES to produce alternative current in the external circuit, where maximum average power can achieve 15-fold enhancement compared to TENG, and the maximum average power can be further boosted by increasing

the supplied voltage, maximum capacitance of C_v , and the frequency of C_v by using a frequency converter. Owing to the allowed low output of lightly contact mode TENG and no-wear DCES, the DCE-TENG displays a low mechanical wear and superior durability with 94% retention charge after 1 000 000 cycles. Furthermore, without the influence of humidity on

charge injection and charge transferring, DCE-TENG exhibits a great humidity resistance with 95% retention value under 90% humidity. This work would be instructive for the enhancement of service life, output performance, and humidity resistance for TENG, which further promotes the commercialization and application of TENG.

4. Experimental Section

Fabrication of TENG: The rotary TENG mainly included a rotor and a stator. For the rotor, the acrylic sheet was used as friction material, which was cut into a disk-shape with radial-arrayed sectors (four in all) that had the same central angle of about 40°, and the diameter of disk-shaped acrylic sheet was 7.5 cm. For the stator, a disk-shaped acrylic sheet was adopted as the substrate, a piece of foam was pasted on the substrate to increase the contact intimacy. After that, a conductive fabric with four complementary sector electrodes stuck onto the surface of foam, where the diameter was 7.5 cm and central angle was 40°. Here, conductive fabric was used as the electrode due to its characteristics of well conductivity (0.002–0.012 $\Omega\text{ m}^{-1}$) and easy cutting. Finally, a layer of Kapton film with thickness of 50 μm adhered on the surface of electrode.

Fabrication of C_v : Each unit of C_v mainly consisted of a pair of electrodes and dielectric layer, where Cu film was used as rotary electrode and stator electrode, air and Kapton film were applied as dielectric layers. For both the rotary electrode and stator electrode, a disk-shaped printed circuit board (PCB) with diameter of 7 cm was used as the supporting substrate, where a predeposited copper film with semicircle shape on the PCB surface was adopted as electrode. A layer of 50 μm Kapton film was adhered on the surface of electrode as dielectric material. For the rotor electrode, there were three small holes with diameter of 6 mm in the center of the circle to fix the rotating shaft. To avoid the contact between rotating shaft and stator electrode, a hole with diameter of 3 cm was perpetrated in the center of stator electrode. Between the two electrodes, there was a certain gap distance created by a spacer with thickness of 1 mm to avoid direct contact of them. Here, ten pairs of electrodes were adopted to obtain a large capacitance.

Characterization and Electrical Measurement: The rotary motion was conducted by a rotational motor (80BL165S75-3130TK0). The short-circuit-current-transferred charges of TENG were tested by a programmable electrometer (Keithley model 6514). The open-circuit voltage of TENG was measured by electrostatic voltmeter (347-3-H-CE). The capacitance of the capacitor and the charging/discharging curves of the self-charging power system were detected by a potentiostat (VSP-300, France). The capacitance of the device with sliding motion was measured by digital graphical multimeter (VC9808). SEM (Nova NanoSEM 450), atomic force microscope (Bruker icon), and optical microscope (GP-660 V) were used to measure the microscopy images of dielectric film surface. Surface roughness tester (TR200) was adopted to examine the surface roughness of dielectric film surface.

COMSOL Simulation: The potential distribution between the complementary electrodes of TENG was calculated using the commercial software COMSOL. The total surface charges of Kapton film and acrylic sheet of rotor were equal, where the surface charge densities of the Kapton film and acrylic sheet were set as 10 and 20 $\mu\text{C m}^{-2}$, respectively.

Supporting Information

Supporting Information is available from the Wiley Online Library or from the author.

Acknowledgements

L.Z., Y.G., and D.L. contributed equally to this work. Research was supported by the National Key R & D Project from Minister of Science

and Technology (Grant No. 2016YFA0202701), the Beijing Municipal Science & Technology Commission (Grant Nos. Z171100000317001, Z171100002017017, Y3993113DF), the National Natural Science Foundation of China (Grant Nos. 61774016, 51432005, 5151101243, 51561145021). Patents were filed based on the research results presented in this paper.

Conflict of Interest

The authors declare no conflict of interest.

Data Availability Statement

Research data are not shared.

Keywords

dual-capacitor enhancement systems, durability, humidity-resistant, triboelectric nanogenerators, ultrarobust

Received: June 26, 2021

Revised: August 10, 2021

Published online:

- [1] K. Dong, X. Peng, J. An, A. C. Wang, J. Luo, B. Sun, J. Wang, Z. L. Wang, *Nat. Commun.* **2020**, *11*, 11.
- [2] T. Jin, Z. Sun, L. Li, Q. Zhang, M. Zhu, Z. Zhang, G. Yuan, T. Chen, Y. Tian, X. Hou, C. Lee, *Nat. Commun.* **2020**, *11*, 12.
- [3] J. Yu, G. Gao, J. Huang, X. Yang, J. Han, H. Zhang, Y. Chen, C. Zhao, Q. Sun, Z. L. Wang, *Nat. Commun.* **2021**, *12*, 10.
- [4] X. Peng, K. Dong, C. Ye, Y. Jiang, S. Zhai, R. Cheng, D. Liu, X. Gao, J. Wang, Z. L. Wang, *Sci. Adv.* **2020**, *6*, eaba9624.
- [5] F. R. Fan, Z. Q. Tian, Z. L. Wang, *Nano Energy* **2012**, *1*, 328.
- [6] Z. L. Wang, J. Chen, L. Lin, *Energy Environ. Sci.* **2015**, *8*, 2250.
- [7] C. Wu, A. C. Wang, W. Ding, H. Guo, Z. L. Wang, *Adv. Energy Mater.* **2019**, *9*, 1802906.
- [8] R. Hinchet, H. J. Yoon, H. Ryu, M. K. Kim, E. K. Choi, D. S. Kim, S. W. Kim, *Science* **2019**, *365*, 491.
- [9] H. Guo, X. Pu, J. Chen, Y. Meng, M. H. Yeh, G. Liu, Q. Tang, B. Chen, D. Liu, S. Qi, C. Wu, C. Hu, J. Wang, Z. L. Wang, *Sci. Rob.* **2018**, *3*, eaat2516.
- [10] Z. L. Wang, *Nature* **2017**, *542*, 159.
- [11] A. Li, Y. Zi, H. Guo, Z. L. Wang, F. M. Fernández, *Nat. Nanotechnol.* **2017**, *12*, 481.
- [12] H. Zou, Y. Zhang, L. Guo, P. Wang, X. He, G. Dai, H. Zheng, C. Y. Chen, A. C. Wang, C. Xu, Z. L. Wang, *Nat. Commun.* **2019**, *10*, 1427.
- [13] J. Wang, S. Li, F. Yi, Y. Zi, J. Lin, X. Wang, Y. Xu, Z. L. Wang, *Nat. Commun.* **2016**, *7*, 12744.
- [14] S. Wang, Y. Xie, S. Niu, L. Lin, C. Liu, Y. Zhou, Z. L. Wang, *Adv. Mater.* **2014**, *26*, 6720.
- [15] J. Wang, C. Wu, Y. Dai, Z. Zhao, A. Wang, T. Zhang, Z. L. Wang, *Nat. Commun.* **2017**, *8*, 88.
- [16] L. Cheng, Q. Xu, Y. Zheng, X. Jia, Y. Qin, *Nat. Commun.* **2018**, *9*, 8.
- [17] W. Liu, Z. Wang, G. Wang, G. Liu, J. Chen, X. Pu, Y. Xi, X. Wang, H. Guo, C. Hu, Z. L. Wang, *Nat. Commun.* **2019**, *10*, 9.
- [18] Y. Liu, W. Liu, Z. Wang, W. He, Q. Tang, Y. Xi, X. Wang, H. Guo, C. Hu, *Nat. Commun.* **2020**, *11*, 8.
- [19] H. Wang, L. Xu, Y. Bai, Z. L. Wang, *Nat. Commun.* **2020**, *11*, 9.

- [20] L. Li, X. Wang, P. Zhu, H. Li, F. Wang, J. Wu, *Nano Energy* **2020**, *70*, 104476.
- [21] H. Guo, Z. Wen, Y. Zi, M. H. Yeh, J. Wang, L. Zhu, C. Hu, Z. L. Wang, *Adv. Energy Mater.* **2016**, *6*, 1501593.
- [22] R. Wen, J. Guo, A. Yu, J. Zhai, Z. L. Wang, *Adv. Funct. Mater.* **2019**, *29*, 1807655.
- [23] Y. Hu, X. Wang, H. Li, H. Li, Z. Li, *Nano Energy* **2020**, *71*, 104640.
- [24] Z. L. Wang, A. C. Wang, *Mater. Today* **2019**, *30*, 34.
- [25] J. Chen, J. Yang, H. Guo, Z. Li, L. Zheng, Y. Su, Z. Wen, X. Fan, Z. L. Wang, *ACS Nano* **2015**, *9*, 12334.
- [26] X. Li, X. Yin, Z. Zhao, L. Zhou, D. Liu, C. Zhang, C. Zhang, W. Zhang, S. Li, J. Wang, Z. L. Wang, *Adv. Energy Mater.* **2020**, *10*, 1903024.
- [27] J. Chen, H. Guo, C. Hu, Z. L. Wang, *Adv. Energy Mater.* **2020**, *10*, 2000886.
- [28] S. Niu, Y. Zhou, S. Wang, Y. Liu, L. Lin, Y. Bando, Z. L. Wang, *Nano Energy* **2014**, *8*, 150.
- [29] Y. Bai, L. Xu, S. Lin, J. Luo, H. Qin, K. Han, Z. L. Wang, *Adv. Energy Mater.* **2020**, *10*, 2000605.
- [30] Y. Li, Z. Zhao, L. Liu, L. Zhou, D. Liu, S. Li, S. Chen, Y. Dai, J. Wang, Z. L. Wang, *Adv. Energy Mater.* **2021**, *11*, 2100050.